NeuroImage 210 (2020) 116533

Contents lists available at ScienceDirect

NeuroImage

journal homepage: www.elsevier.com/locate/neuroimage

Diffusion time dependency along the human corpus callosum and exploration of age and sex differences as assessed by oscillating gradient spin-echo diffusion tensor imaging

Pascal Tétreault [a], Kevin D. Harkins [b], Corey A. Baron [c], Rob Stobbe [a], Mark D. Does [b], Christian Beaulieu [a,*]

[a] Department of Biomedical Engineering, Faculty of Medicine and Dentistry, University of Alberta, Edmonton, AB, Canada
[b] Institute of Imaging Science and Department of Biomedical Engineering, Vanderbilt, University, Nashville, TN, USA
[c] Department of Medical Biophysics, Western University, London, ON, Canada

ARTICLE INFO

Keywords:
DTI
Corpus callosum
OGSE
Aging
Sex
Monte Carlo simulation

ABSTRACT

Conventional diffusion imaging uses pulsed gradient spin echo (PGSE) waveforms with diffusion times of tens of milliseconds (ms) to infer differences of white matter microstructure. The combined use of these long diffusion times with short diffusion times (<10 ms) enabled by oscillating gradient spin echo (OGSE) waveforms can enable more sensitivity to changes of restrictive boundaries on the scale of white matter microstructure (e.g. membranes reflecting the axon diameters). Here, PGSE and OGSE images were acquired at 4.7 T from 20 healthy volunteers aged 20–73 years (10 males). Mean, radial, and axial diffusivity, as well as fractional anisotropy were calculated in the genu, body and splenium of the corpus callosum (CC). Monte Carlo simulations were also conducted to examine the relationship of intra- and extra-axonal radial diffusivity with diffusion time over a range of axon diameters and distributions.

The results showed elevated diffusivities with OGSE relative to PGSE in the genu and splenium (but not the body) in both males and females, but the OGSE-PGSE difference was greater in the genu for males. Females showed positive correlations of OGSE-PGSE diffusivity difference with age across the CC, whereas there were no such age correlations in males. Simulations of radial diffusion demonstrated that for axon sizes in human brain both OGSE and PGSE diffusivities were dominated by extra-axonal water, but the OGSE-PGSE difference nonetheless increased with area-weighted outer-axon diameter. Therefore, the lack of OGSE-PGSE difference in the body is not entirely consistent with literature that suggests it is composed predominantly of axons with large diameter. The greater OGSE-PGSE difference in the genu of males could reflect larger axon diameters than females. The OGSE-PGSE difference correlation with age in females could reflect loss of smaller axons at older ages. The use of OGSE with short diffusion times to sample the microstructural scale of restriction implies regional differences of axon diameters along the corpus callosum with preliminary results suggesting a dependence on age and sex.

1. Introduction

The inferences made on neural microstructure from diffusion MRI depend on the time that the diffusing water molecules interact with their microscopic surroundings. The manipulation of this diffusion time to interrogate restricted diffusion by barriers in biological tissue was appreciated early on in excised muscle, which was assessed using repeated bipolar gradient pairs or stimulated-echo to enable shorter or longer diffusion times, respectively, compared to the typical pulsed gradient spin-echo (PGSE) diffusion MRI sequence (Tanner, 1979). Signal dependencies on various diffusion times over tens of milliseconds were the crux of an early white matter model (Stanisz et al., 1997) and are part of the experimental methodology for axon diameter estimation by diffusion imaging techniques such as AxCaliber (Assaf et al., 2008) and ActiveAx (Alexander et al., 2010). However, these techniques used diffusion times that were relatively long given the size of the restrictive

* Corresponding author. Department of Biomedical Engineering, University of Alberta, 1098 Research Transition Facility, University of Alberta, Edmonton, AB, T6G 2V2, Canada.
E-mail address: christian.beaulieu@ualberta.ca (C. Beaulieu).

https://doi.org/10.1016/j.neuroimage.2020.116533
Received 4 October 2019; Received in revised form 6 January 2020; Accepted 9 January 2020
Available online 11 January 2020

boundaries (i.e. axon size), which limits the ability to distinguish smaller axons although this can be improved with stronger gradients (Drobnjak et al., 2016; Dyrby et al., 2013; Huang et al., 2015; Nilsson et al., 2017). One of the earlier Monte Carlo simulations showed that <10 ms diffusion times should yield marked changes of measured apparent diffusion parameters in anisotropic tissue (Szafer et al., 1995). This was observed experimentally for diffusion times as short as ~2 ms in excised nerve (Beaulieu and Allen, 1996) and healthy rat brain (Niendorf et al., 1994).

Short diffusion times (e.g. <10 ms) are made possible for MRI using oscillating gradient spin-echo (OGSE) waveforms (Schachter et al., 2000). Preclinical studies of the brain in vivo have shown elevated diffusion with progressively greater OGSE oscillation frequencies (i.e. shorter diffusion times) in rat cortical gray matter (Does et al., 2003) and mouse white matter (Aggarwal et al., 2012), notably also showing greater increases with frequency in global ischemia and demyelination, respectively. The greater sensitivity of OGSE to restrictive compartment sizes has been demonstrated in various ex vivo samples of brain, nerve, and spinal cord where even higher frequencies and shorter diffusion times are possible with strong gradients (Kakkar et al., 2018; Lundell et al., 2015; Portnoy et al., 2013; Shemesh et al., 2013; Xu et al., 2014). The implementation of this approach on human MRI scanners is more challenging due to weaker gradient systems limiting both frequency and b-value. The first human OGSE studies showing a dependence of diffusion metrics on short diffusion times down to ~4 ms were on the genu/splenium of corpus callosum in 4 subjects with b = 200 s/mm^2 and 63 Hz (Van et al., 2014) and on multiple white matter tracts in 7 subjects using the full tensor with b = 300 s/mm^2 and 50 Hz (Baron and Beaulieu, 2014). The greater mean, parallel and perpendicular diffusivities that were observed at short diffusion times result from the water molecules experiencing less restrictive barriers in that time. Another human OGSE study showed that the slope of the diffusion coefficient plotted linearly as a function of OGSE frequency was different along the length of the corpus callosum in 6 subjects; steeper slopes (i.e. greater OGSE-PGSE differences) in the same paper were related to larger axon diameters as shown experimentally in excised rat spinal cord (Xu et al., 2016). This time dependence of diffusivities is also observed over much longer diffusion times using stimulated echo diffusion methods in human brain (e.g. up to 180 ms in (De Santis et al., 2016) and 600 ms in (Fieremans et al., 2016)).

The corpus callosum (CC) is a common white matter tract for diffusion microstructure studies given its large dimensions, role in interhemisphere connectivity, and histology-based variability of axon diameters/density from anterior (genu) to posterior (splenium) across species such as rat (Barazany et al., 2009), macaque (Caminiti et al., 2013; Stikov et al., 2015) and humans (Aboitiz et al., 1992). This latter de facto human autopsy paper on 10 males and 10 females analyzed with light microscopy reports that by far the most populous axons are less than 1 μm (uncorrected for fixation shrinkage) in diameter with a greater density in the genu and splenium (Aboitiz et al., 1992). However, larger axons are also observed in smaller number, primarily in the body followed by the splenium then the genu (see (Aboitiz and Montiel, 2003) for a pictorial distribution of the axons of the corpus callosum). The similarity of the genu and splenium both being different than the body is reported commonly in model-based diffusion MRI microstructure studies, namely low-high-low for axon diameter and high-low-high for axon density for genu-body-splenium in humans (Alexander et al., 2010; De Santis et al., 2016; Fick et al., 2016; Huang et al., 2015), macaque (Alexander et al., 2010; Dyrby et al., 2013), rats (Barazany et al., 2009), and mice (Sepehrband et al., 2016; Shemesh et al., 2015).

Males and females have shown similar distributions of axon size across the corpus callosum in the previously mentioned autopsy study (Aboitiz et al., 1992). However, lab grown human male axons have been shown to have a larger cross-sectional area than human female axons (Dolle et al., 2018) and bigger axons are reported in the splenium of the CC for male rats (Pesaresi et al., 2015). The hypothesis here is that males would have greater diffusion time dependency than females if their axons were larger, but sex/gender has not been factored into the limited number of small sample OGSE studies of human brain. Other MRI measures such as relaxivity and magnetization transfer have shown sex differences in the human corpus callosum (Björnholm et al., 2017).

Aboitiz et al. replotted their original 1992 data as a function of age over 25–68 years separated by sex, and showed that there was an increase of larger axons with age in both sexes although there were sex differences depending on CC region (Aboitiz et al., 1996). A loss of smaller axons and shift to larger axons with age has been observed with microscopy in rodent (Stahon et al., 2016; Yang et al., 2009) and human autopsy studies (Marner et al., 2003; Tang et al., 1997). Using an imaging protocol modeled on an AxCaliber type acquisition (Fan et al., 2018), a 300 mT/m "Connectom gradient" study in 36 healthy adults aged 22–72

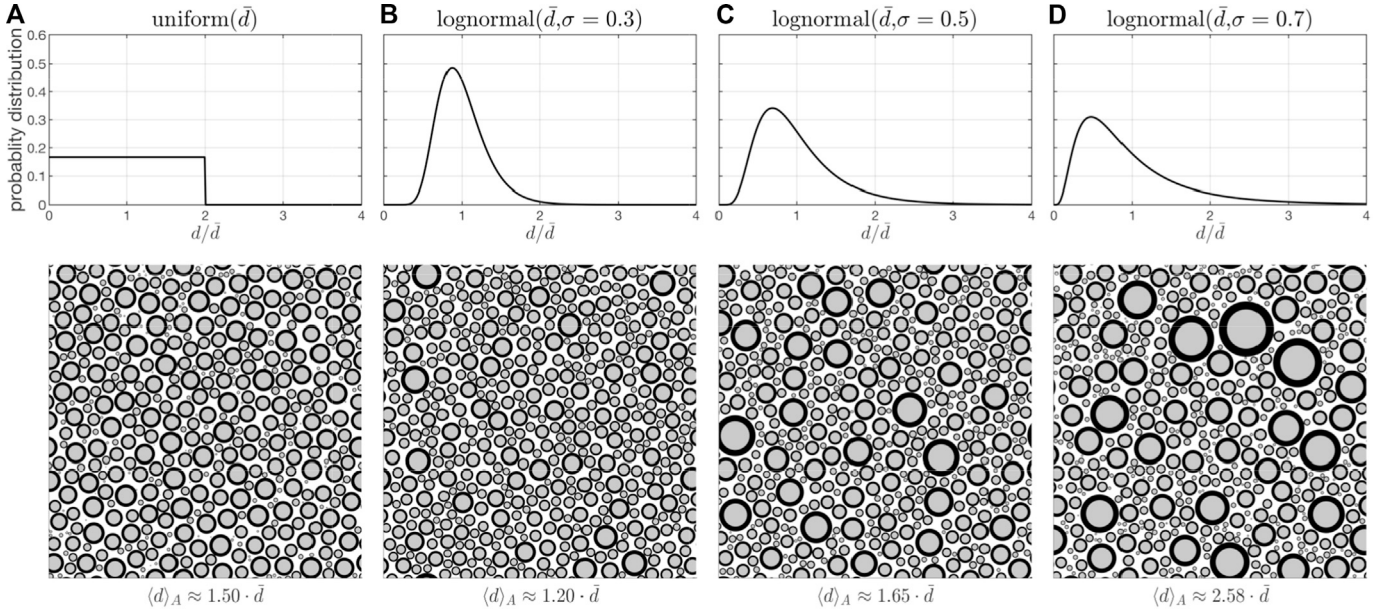

Fig. 1. Example axon size distributions from (A) uniform, (B) lognormal with standard deviation of $\log(d) = 0.3$, (C) lognormal with standard deviation of $\log(d) = 0.5$ and (D) lognormal with standard deviation of $\log(d) = 0.7$ distribution. Distributions are parameterized with arithmetic mean outer axon diameter, $\bar{d}$, and EVF = 0.3. These distributions result in larger area-weighted mean axon diameters d_A of $\approx 1.50\bar{d}$, $1.20\bar{d}$, $1.65\bar{d}$ and $2.58\bar{d}$, respectively.

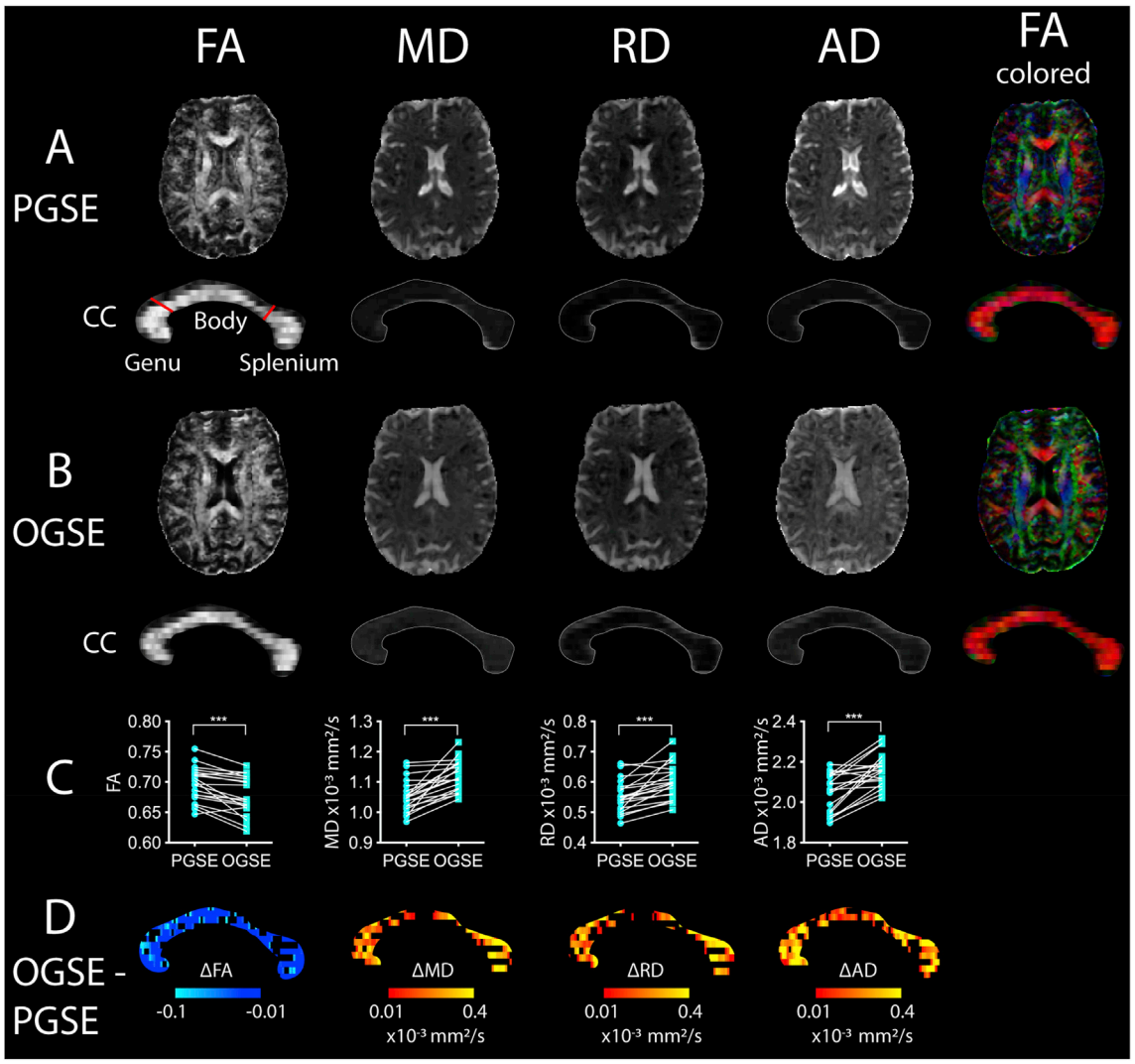

Fig. 2. Example maps of FA, MD, RD, AD and FA color-coded with principal eigenvector direction from a 34-year-old male showing comparable images/maps using (A) long diffusion time PGSE (Δ_{eff} = 40 ms, b = 300 s/mm^2) and (B) short diffusion time OGSE (50 Hz, Δ_{eff} = 4 ms, b = 300 s/mm^2). (C) Over the whole CC, pairwise comparison in all 20 participants showed significant decreases in FA and increases in all diffusivities with OGSE (***p < 0.001). (D) The difference maps (OGSE - PGSE) show heterogeneity in either decreases (blue tones, present in FA), increases (red tones, present in diffusivities) across this single sagittal slice of the CC. Note that any black voxels from these maps reflect changes outside of the prescribed range (either no or excessive changes); these voxels were only excluded to facilitate visualization but are included in subsequent analysis.

years showed age-related increases of axon diameter index and decreases of axon density primarily in the genu (Fan et al., 2019). The hypothesis here is that aging would be associated with greater diffusion time dependency as the relative axon areas get larger with age, but OGSE studies have not factored age into account yet.

The purpose of the present study is to evaluate if the three primary corpus callosum sub-regions demonstrate a sex or age related diffusion time dependence of the diffusion tensor metrics (axial (AD), radial (RD), and mean diffusivities (MD), and fractional anisotropy (FA)). Our previous dataset (Baron and Beaulieu, 2014) has been expanded to include both younger and older subjects to span an age range of 20–73 years, equally distributed between males (n = 10) and females (n = 10), using both short (4 ms, 50 Hz OGSE) and long (40 ms, PGSE) diffusion times. To support our in vivo experiments, 2D Monte Carlo simulations were performed to evaluate the effect of axon diameter with different distributions and extracellular volume fraction on the difference of radial diffusivity between OGSE and PGSE.

2. Methods

2.1. Participants

Twenty healthy volunteers aged 20–73 years old (10 females, 38.0 ± 16.5, 21–73 years; 10 males; 37.7 ± 15.9, 20–67 years) with no self-reported history of neurological or psychiatric disease or brain injury underwent an MRI session. This study was approved by the Health Research Ethics Board of the University of Alberta. All participants gave written informed consent.

2.2. Scanning protocol

DTI scans with short and typical effective diffusion times (Δ_{eff}) were acquired using cosine OGSE 50 Hz (Δ_{eff} = 4.1 ms as calculated in (Parsons et al., 2003)) and PGSE (Δ_{eff} = 40 ms, gradient lobe width δ = 3.9 ms, gradient lobe separation Δ = 41.3 ms) on a Varian Inova 4.7 T MRI using an in-house developed sequence as detailed in (Baron and

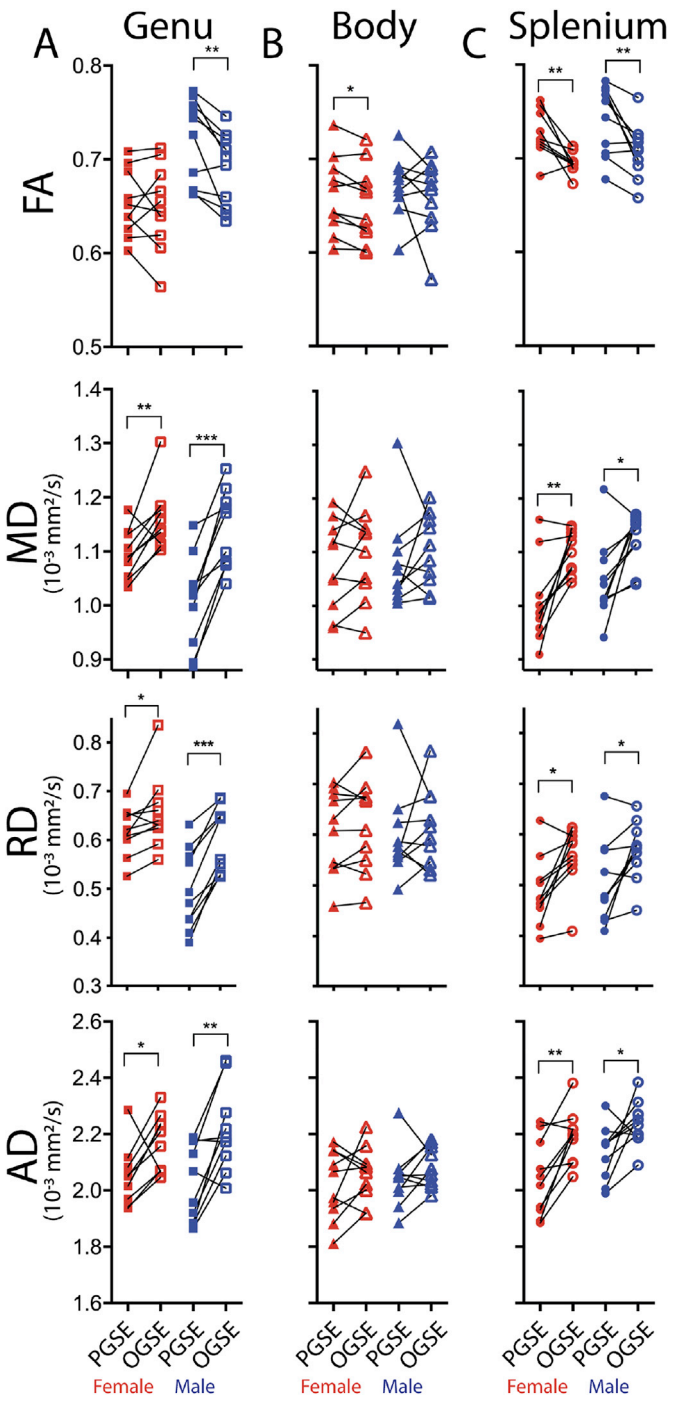

Fig. 3. Comparison of PGSE and OGSE-derived diffusion parameters in subdivisions of the corpus callosum (A – genu, B – body, C – splenium) in females (n = 10, red) and males (n = 10, blue) shown paired per individual. The (A) genu and (C) splenium showed significant differences for nearly all parameters (FA decreases, MD/AD/RD increases) between PGSE and OGSE for both females and males, whereas the (B) body showed nearly no consistent OGSE/PGSE differences across either group. *p < 0.05, **p < 0.01, ***p < 0.001.

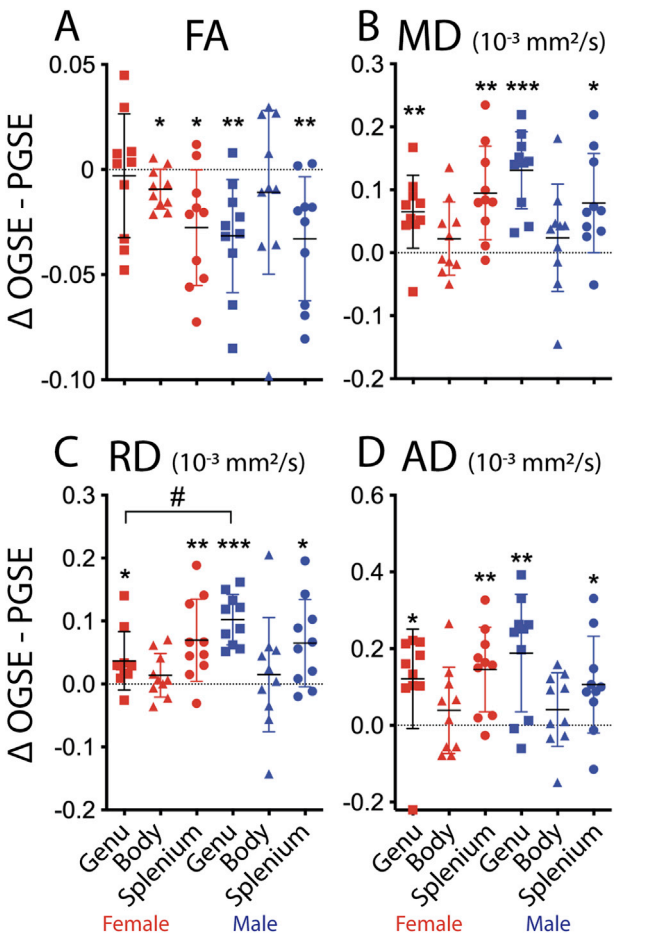

Fig. 4. OGSE-PGSE absolute difference (mean±SD shown) of (A) FA, (B) MD, (C) RD, and (D) AD for three corpus callosum subregions in females (red, n = 10) and males (blue, n = 10) shown per individual. The genu and splenium showed significant OGSE-PGSE differences in nearly all parameters for both sexes. The only sex-specific difference was in the genu which showed a greater RD OGSE increase relative to PGSE in males than females. The body shows no MD, RD, or AD dependence on diffusion time, and only a very small 0.01 reduction of FA in females between OGSE and PGSE. * (for differences from 0) or # (males versus females) p < 0.05, **p < 0.01, ***p < 0.001.

Beaulieu, 2014). It is worth noting that the effective diffusion time for OGSE sequences is model-dependent (Lemberskiy et al., 2017; Novikov and Kiselev, 2010) and, accordingly, all simulations described later used the actual gradient waveforms implemented in this study without any of the simplifying assumptions used to estimate diffusion time. The following parameters were used for data acquisition: scan time of either 5 min each for 20 2.5 mm axial slices over 5 cm centered on the corpus callosum (n = 8) or 10 min each for 40 2.5 mm slices over 10 cm (n = 12); 2D single-shot EPI with R = 2 GRAPPA (4 elements receive coil); partial Fourier 6/8; TR = 12.5 s; TE = 110 ms; FOV = 24 cm; 2x2x2.5 mm^3; 6 averages; b = 300 s/mm^2; 6 gradient directions to maximize b value for minimum TE. The 50 Hz OGSE protocol used two periods per gradient waveform (for a total of four: two before and two after the 180° RF pulse) and both OGSE and PGSE protocols were performed with a maximum gradient of 57.5 mT/m per channel. A subset of 7 of these subjects (with the 40 slice, 10 min protocol) was analyzed in a previous publication (not aging focused) where scanning parameters are presented with more details (Baron and Beaulieu, 2014). There was limited slice coverage of 8 of the participants since they were part of a control group for a study on multiple sclerosis that had already underwent over 1 h of scanning (focused on sodium MRI) and hence the OGSE/PGSE protocol was kept short with a focus on the corpus callosum. Both 20 and 40 slice protocols covered the full extent of the corpus callosum reported here.

2.3. DTI analysis

The diffusion tensor data was processed using ExploreDTI and its

Table 1
Mean difference between OGSE and PGSE for FA, MD, RD and AD in the genu, body and splenium of the corpus callosum in females (n = 10) and males (n = 10).

OGSE - PGSE	Sex	Genu			Body			Splenium		
		Absolute	Relative	p-value	Absolute	Relative	p-value	Absolute	Relative	p-value
FA	Females	−0.003	−0.5%	0.4	**−0.01**	**−1.4%**	**0.013**	**−0.03**	**−3.7%**	**0.008**
	Males	**−0.03**	**−4.3%**	**0.005**	−0.01	−1.5%	0.212	**−0.03**	**−4.3%**	**0.008**
MD	Females	$\mathbf{0.07x10^{-3}}$	**6.0%**	**0.006**	0.02×10^{-3}	2.2%	0.421	$\mathbf{0.09x10^{-3}}$	**9.9%**	**0.006**
	Males	$\mathbf{0.13x10^{-3}}$	**13.3%**	**0.0002**	0.02×10^{-3}	2.6%	0.421	$\mathbf{0.08x10^{-3}}$	**7.9%**	**0.011**
RD	Females	$\mathbf{0.04x10^{-3}}$	**5.9%**	**0.033**	0.01×10^{-3}	2.3%	0.486	$\mathbf{0.07x10^{-3}}$	**15.4%**	**0.016**
	Males	$\mathbf{0.10x10^{-3}}$	**21.8%**	**0.00004**	0.02×10^{-3}	3.6%	0.643	$\mathbf{0.07x10^{-3}}$	**14.6%**	**0.016**
AD	Females	$\mathbf{0.12x10^{-3}}$	**6.1%**	**0.016**	0.04×10^{-3}	2.2%	0.313	$\mathbf{0.15x10^{-3}}$	**7.4%**	**0.005**
	Males	$\mathbf{0.19x10^{-3}}$	**9.6%**	**0.007**	0.04×10^{-3}	2.2%	0.313	$\mathbf{0.11x10^{-3}}$	**5.2%**	**0.026**

FA: Fractional Anisotropy, MD: Mean Diffusivity, RD: Radial Diffusivity, AD: Axial Diffusivity, Absolute: absolute difference (in mm^2/s for MD, RD and AD), Relative: percent difference relative to PGSE (OGSE-PGSE)/PGSE, p: FDR corrected p-values for absolute difference between OGSE and PGSE. Significant differences between OGSE and PGSE are identified in bold.

imbedded set of tools (version 4.8.6). Briefly, data was first corrected for Gibbs ringing artifacts (Perrone et al., 2015), followed by rigid body motion with elastix and eddy current corrections (Klein et al., 2010; Leemans and Jones, 2009; Shamonin et al., 2013). The tract of focus was the central portion of the corpus callosum (partly given the limited inferior/superior coverage here), which was segmented using tractography-based 3D ROIs. Based on our previous publication (Baron and Beaulieu, 2014), each CC subregion tract was extracted based on a manually drawn seed ROI of the CC located in the middle sagittal reconstructed slice and one end ROI located right before the beginning of the main upward curvature in each hemisphere (i.e. on the color FA map coded for fiber direction, end ROIs were placed when the y-plane slice was reaching inferior to superior fibers). The mean tract length of each CC segment was 13.7 ± 1.5 mm for the body, 11.1 ± 1.2 mm for the genu and 14.1 ± 1.7 mm for the splenium. Deterministic tracking used an FA threshold of 0.2 and a maximum angulation threshold of 30°. Fiber tract segments for genu, body and splenium were made for each subject for PGSE and OGSE protocols. The diffusion parameters of fractional anisotropy (FA), mean (MD), axial (AD), and radial diffusivities (RD) were averaged over the entire tract region.

2.4. Statistical image analysis

Analyses were performed using IBM SPSS Statistics for Mac, version 24.0.0.1. Armonk, NY:IBM Corp, and Graph Pad Prism for Mac, version 8.1.2, San Diego, California. The four diffusion parameters were compared between OGSE and PGSE in the three sub-regions of the corpus callosum for males and females separately. Based on the Shapiro-Wilk test for normality, most of these distributions were normally distributed (40/48) and a paired *t*-test was therefore used, followed by a correction for false discovery rate (FDR) with a corrected p-value threshold of 0.033. In addition, the absolute OGSE-PGSE difference of the diffusion parameters were assessed per CC region with a one sample *t*-test (compared to 0) with FDR correction (corrected p-value threshold of 0.025) and a one-way ANOVA was further used to compare between males and females in a region-wise manner. The difference of diffusion parameters between OGSE and PGSE were assessed for linear correlations versus age for males and females separately. A correction for FDR was further applied on the correlation results, with a corrected p-value threshold of 0.01.

2.5. Monte Carlo simulations

In order to investigate the microstructural characteristics that affect RD, experiments were simulated using the same PGSE and OGSE diffusion-weighting gradient waveforms outlined above, applied perpendicular to axons with various geometries. As previously described (Harkins and Does, 2016), axons were modeled as two concentric circles, defined by an outer diameter (d) and g-ratio (g). For each simulation, N = 500 axons were uniformly distributed into an arena with a defined extra-axonal volume fraction (EVF) and with periodic boundary conditions (Hall and Alexander, 2009). Each axon diameter, d_i for $i = 1$ to N, was randomly sampled from a given probability distribution, either uniform $(\overline{d})$ or lognormal $(\overline{d}, \sigma)$, where $\overline{d}$ was the arithmetic mean axon diameters and σ was the standard deviation of $\log(d)$ (Buzsaki and Mizuseki, 2014). Simulations were performed using every combination of EVF = 0.3, 0.4, 0.5, 0.6, 0.7, $\overline{d}$ = 0.5, 0.8, 1.0, 1.5, 2.0, 3.0, 4.0, 6.0, 8.0, 10.0 μm, and (for lognormal axon diameter distributions) σ = 0.3, 0.5, 0.7. For each set of sampled axon diameters, the area-weighted outer axon diameter, d_A, was calculated as

$$d_A = \frac{\sum_i d_i^3}{\sum_i d_i^2}.$$

Simulation results were tabulated only for scenarios of $d_A < 12$ μm, because larger values were considered unrealistic for human corpus callosum. Fig. 1 shows four examples of axon diameter distributions, one uniform and three lognormal, with mean axon diameter, $\overline{d}$, and EVF = 0.3. Note that while the $\overline{d}$ is constant across these distributions, the computed area-weighted axon diameter, d_A, increases with inclusion of larger axon sizes. The length of the square simulation arena, L_x, varied with EVF, $\overline{d}$, and axon distribution, with a range of 12.4 to 559 μm, and an average length of 148 μm. On average, L_x was 4x greater than the root mean squared displacement of extra-axonal water diffusion (RMSD). While the RMSD approached L_x for geometries with the smallest axon sizes, these geometries exhibited the smallest difference in OGSE and PGSE RD. Therefore, we expect any correlations in radial diffusivity (Burcaw et al., 2015) caused by the periodic boundary condition to have a minimal effect on the simulated results.

All simulations were run with a constant $g = 0.7$ (Chomiak and Hu, 2009) and free water diffusion coefficient, $D_0 = 3.0 \times 10^{-3}$ mm^2/s. Myelin water, inter-compartmental water exchange, and relaxation were neglected. The number of spins simulated was set to 200,000, providing a lower bound on the SNR of the simulated signal ≈450 (Harkins and Does, 2016). No additional thermal noise was added to the simulated signals. Gradient waveforms were simulated with a time step of 3 μs, which was empirically tested to not bias the simulations, resulting in a spatial step of ≈0.19 μm at each time step in a random orientation, and 36893 total steps. Simulated signals and subsequently calculated RD values were tabulated independently for intra-axonal and extra-axonal compartments as well as in total. Simulations were implemented in CUDA and MATLAB, and run on a Linux computer with a GeForce GTX Titan GPU. The entire set of simulations completed in 2–3 days.

3. Results

3.1. PGSE and OGSE DTI in human brain

Representative maps of fractional anisotropy (raw and color encoded for principal eigenvector direction) and mean, radial, and axial

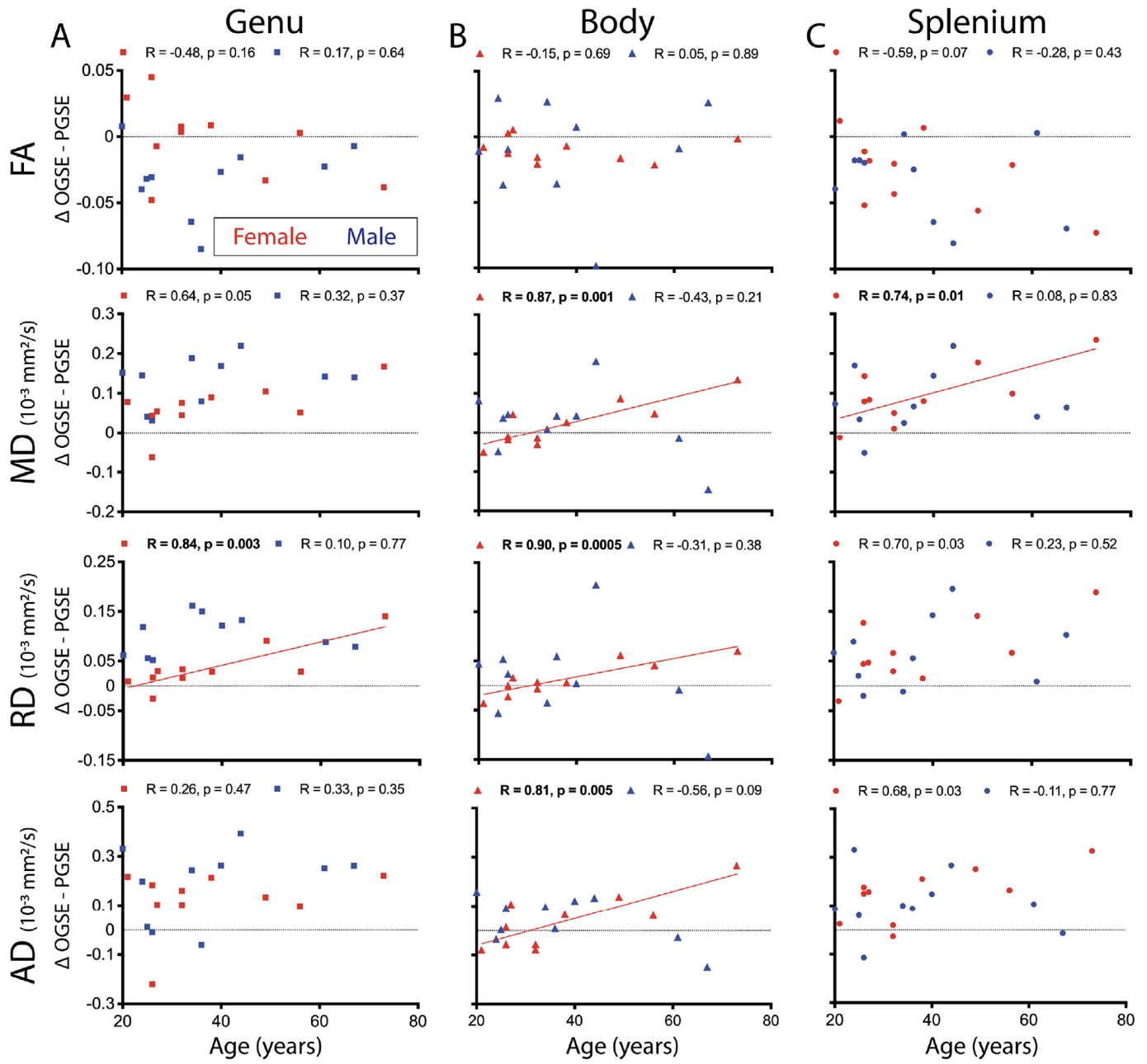

Fig. 5. Linear age dependence of OGSE versus PGSE diffusion parameter absolute differences for all three corpus callosum sub-regions in females and males separately. Significant OGSE-PGSE increases with age were observed for (A) RD in the genu, (B) MD/RD/AD in the body, and (C) MD in the splenium of the female group. However, the 7 women under 40 years are scattered around zero difference and the correlation appears driven by the greater OGSE-PGSE diffusivity difference in the 3 women aged 49, 56, and 73 years. In contrast, males did not show any significant correlations with age. Only significant correlations surviving FDR correction (p-value threshold of 0.01) are displayed with best fit lines.

diffusivities show overall comparable quality between PGSE (Fig. 2A) and OGSE (50 Hz) (Fig. 2B). A notable qualitative difference between the two scans is the increased signal of the cerebrospinal fluid (CSF) on only the PGSE due to turbulent CSF flow, as shown before (Baron and Beaulieu, 2014; Wu and Zhang, 2017). When evaluated across the whole CC for the entire group (Fig. 2C), OGSE showed significant paired decrease for FA when compared to PGSE (Mean FA: 0.70 ± 0.03 for PGSE vs 0.68 ± 0.03 for OGSE, $p = 0.00012$) and all diffusivity parameters showed significant paired increases for OGSE (Mean MD: 1.05 ± 0.05 × 10^{-3} mm^2/s for PGSE vs 1.12 ± 0.05 × 10^{-3} mm^2/s for OGSE, $p = 0.00002$; Mean RD: 0.55 ± 0.05 × 10^{-3} mm^2/s for PGSE vs 0.60 ± 0.06 × 10^{-3} mm^2/s for OGSE, $p = 0.00010$ and Mean AD: 2.05 ± 0.10 × 10^{-3} mm^2/s for PGSE vs 2.16 ± 0.08 × 10^{-3} mm^2/s for OGSE, $p = 0.00004$). The OGSE - PGSE difference map (Fig. 2D, shown in the CC only for one mid-sagittal slice) illustrates the heterogeneous diffusivity differences with diffusion time along the CC.

3.2. Sex differences of OGSE versus PGSE

The primary focus here was on the three sub-regions of the CC with participants separated by sex. All the diffusivity parameters in the genu (Fig. 3A) and splenium (Fig. 3C) showed significant paired increases on OGSE relative to PGSE in both females and males. In contrast, the body of the corpus callosum had no significant OGSE-PGSE MD, RD, or AD differences in either females or males (Fig. 3B). FA was lower with OGSE in the genu only for males, in the body only for females and in the splenium

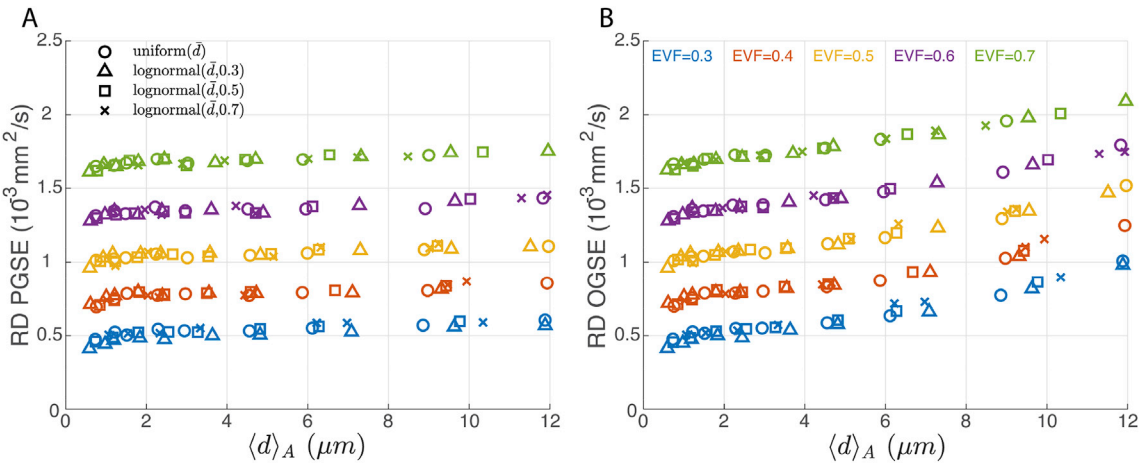

Fig. 6. Radial diffusivity (RD) values obtained from Monte Carlo simulations for (A) PGSE and (B) OGSE (50 Hz) for four axon size distributions and five EVFs. Both PGSE and OGSE RD are sensitive to changes in EVF while only OGSE RD increases markedly with greater area-weighted mean outer axon diameter d_A.

for both males and females (Fig. 3 top row and Fig. 4A). Also, as the difference could be expected in both males and females, all the subjects were taken together (n = 20), but there was no difference in the body for any of the metrics. Relative to males, the genu in females demonstrated a smaller increase of OGSE over PGSE for RD (Fig. 4C). In contrast, the splenium showed comparable increases for both sexes of OGSE over PGSE for MD and RD. AD was similarly elevated for females and males on OGSE over PGSE for the genu and splenium (Fig. 4D). All diffusion parameter absolute and percent differences with respective p-values are presented in Table 1 for the three sub-regions. Overall in the genu and splenium in the combined group, the significant percentage changes of OGSE relative to PGSE are greater for RD (+5.9% to +21.8%) than AD (+5.2% to +9.6%), leading to a small reduction of FA (−3.7% to −4.3%) and moderate increases of MD (+6.0% to +13.3%).

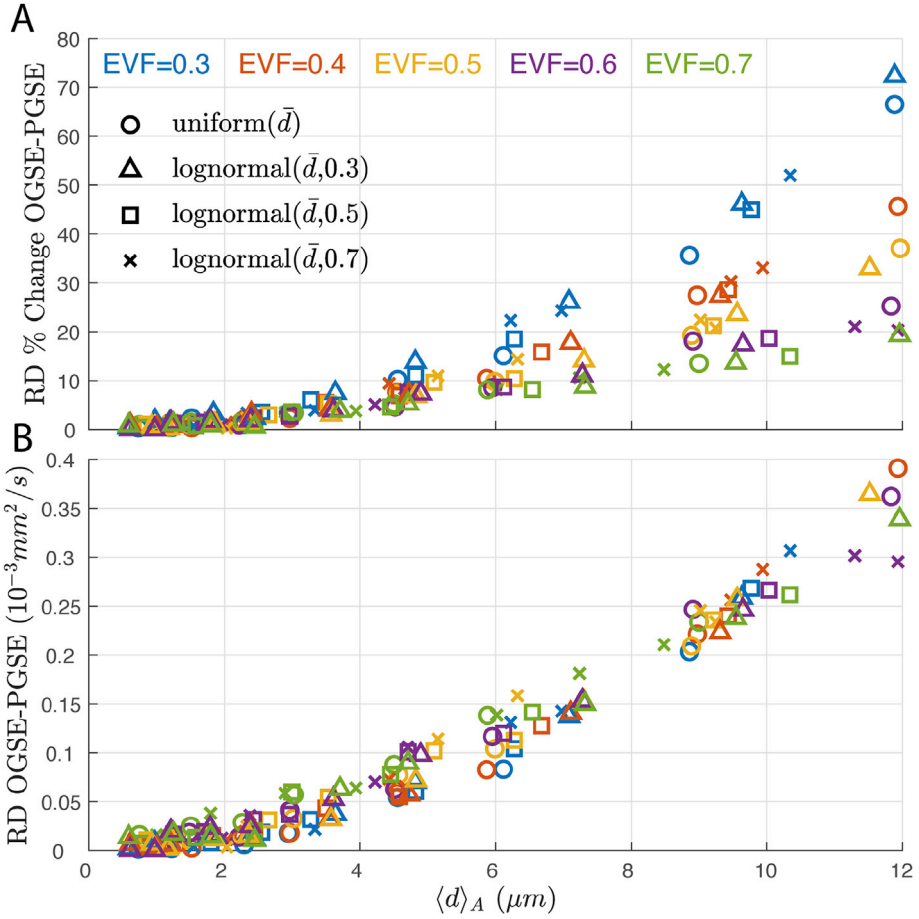

Fig. 7. The (A) relative and (B) absolute difference between RD simulated from PGSE and OGSE (50 Hz) are plotted versus area-weighted mean outer axon diameter d_A. Low EVF and high d_A generates the highest relative (%) OGSE - PGSE difference, while absolute OGSE - PGSE difference is proportional to d_A increase, but is insensitive to changes in EVF.

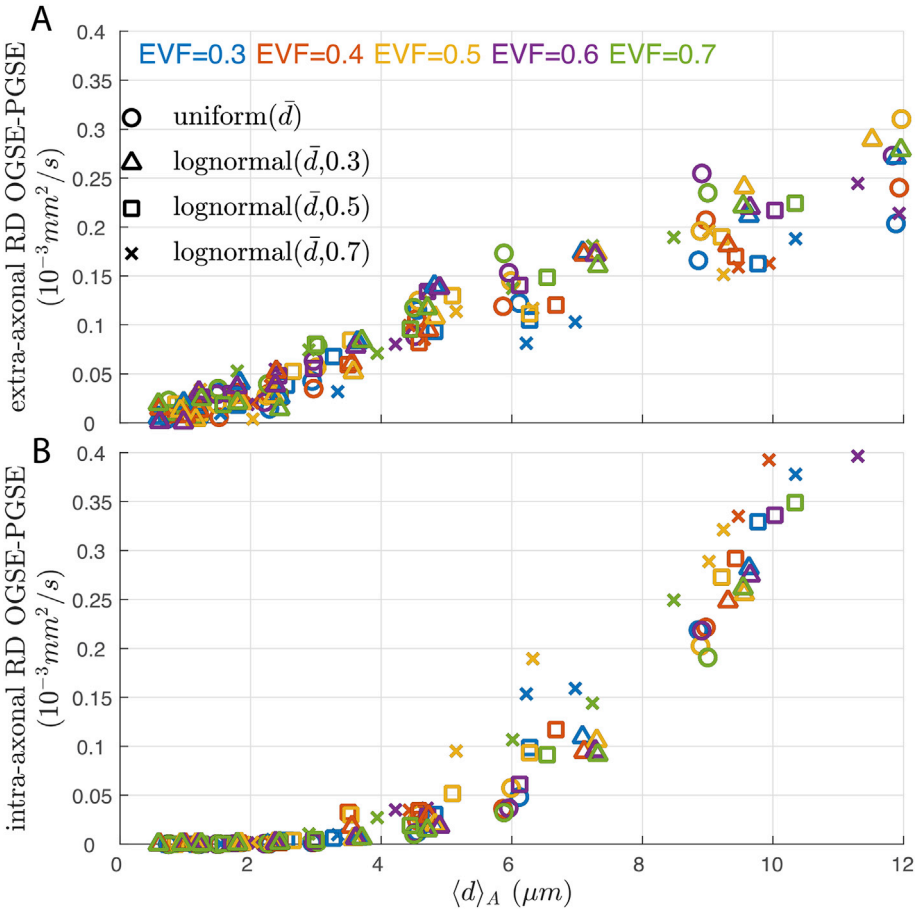

Fig. 8. The absolute difference between RD simulated from OGSE and PGSE of the (A) extra-axonal and (B) intra-axonal space separately. Extra-axonal RD OGSE-PGSE is larger than intra-axonal RD OGSE-PGSE for $d_A < 6$ μm.

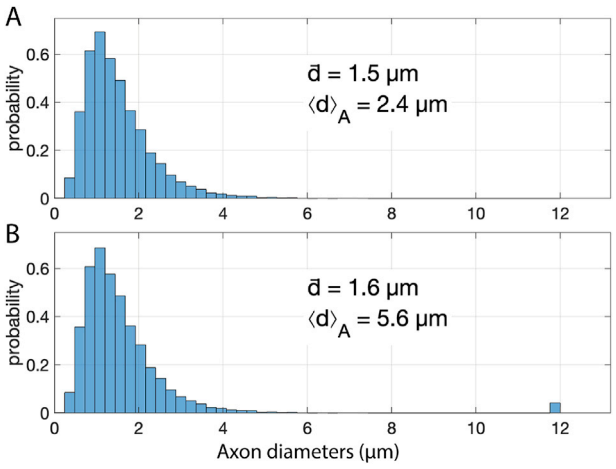

Fig. 9. Example of lognormal distributions with a (A) mean outer diameters of 1.5 μm ($\sigma = 0.5$) producing an area-weighted mean axon diameter d_A of 2.4 μm. The same distribution is presented in (B) including 1% of 12 μm diameters axons, producing a minimal mean diameter increase of 0.1 μm, while the resultant area-weighted mean axon diameter d_A more than doubles.

3.3. Correlation of OGSE versus PGSE difference with age

The age span of 20–73 years of age permitted an opportunity for preliminary analysis of whether the difference of the diffusion tensor parameters between short diffusion time OGSE and long diffusion time PGSE was altered with adult aging in a separate analysis of females and males, admittedly with a small sample size of 10 per group. Over the entire combined group, there was no significant correlation of absolute change of OGSE versus PGSE with age after correction for multiple comparison, but it correlated positively with age for MD (body/splenium), RD (genu, body), and AD (body) in females (Fig. 5). No age correlations were found in males. These age correlations were driven by larger OGSE-PGSE differences in the 3 older females (49, 56, 73 years). The males had consistent OGSE-PGSE differences across the adult age span for the genu and splenium, whereas the body showed no consistent diffusion time differences for any age in males. The OGSE-PGSE difference for FA did not correlate with age in any corpus callosum region for either sex. However, as an age effect could be expected for both males and females, an ANCOVA analysis was performed while setting age as a covariate and sex as a fixed factor. This analysis revealed a significant difference in the slopes of males and females only for body AD and MD while body RD, genu RD and splenium MD were not significant (see Supplemental Table S1 for statistical details).

3.4. Monte Carlo simulations of axonal distribution with PGSE and OGSE

To help interpret the experimental results in human brain using OGSE and PGSE, 2D Monte Carlo simulations were performed on various axonal distributions. Simulation results shown in Fig. 6 demonstrate that for all four axon diameter distributions, simulated RD increased markedly with increasing EVF, as expected. For a given EVF, RD from PGSE was nearly constant over the range of d_A from 0.5 to 12 μm, while OGSE provided a greater dependence of RD on d_A. These absolute RD trends were relatively independent of EVF and axon size distribution.

For all four axon diameter distributions and five EVF values, the relative and absolute differences between RD from OGSE and PGSE is plotted versus d_A in Fig. 7. The difference in RD (OGSE – PGSE) began to deviate from zero at $d_A \approx$ 3 μm, and then continued to increase with increasing d_A. The relative difference in RD depended upon d_A and EVF (top row), but the absolute difference in RD OGSE-PGSE was nearly independent of EVF and axon distribution over the 1–12 μm d_A domain. Looking at the compartment specific extra- and intra-axonal RD differences (Fig. 8), we see that *both* water compartments report on d_A and that for $d_A < 5$ μm, the total OGSE-PGSE difference is driven almost entirely by extra-axonal water signals. In Supplemental Fig. 1, these same data is plotted vs d_A^2, which may be a better indicator of extra-axonal diffusion (Burcaw et al., 2015). When linking these simulated differences to the human experimental observations above, the results suggest a similar mean area-weighted outer axon diameter of 3.5–5 μm for both females and males in the splenium, while the genu differences suggest a mean area-weighted outer axon diameter of 2–3 μm for females and 5–6 μm for males.

4. Discussion

This study focused on the corpus callosum of 20 healthy participants and is an extension of our initial publication showing the feasibility of OGSE DTI in human brain where we demonstrated diffusion time dependence in multiple white matter tracts even with such low b values (Baron and Beaulieu, 2014). There are four new key findings to be discussed below: (i) the genu and splenium of the corpus callosum show consistent OGSE-PGSE differences but the body did not, (ii) these differences were similar between males and females with the exception of the genu that showed greater radial diffusivity increases at short diffusion time in males, (iii) only females showed linear increases of the percent OGSE-PGSE difference with age in the various corpus callosum sub-regions, and (iv) Monte Carlo simulations showed that the absolute difference in OGSE – PGSE radial diffusivity depends primarily on the area-weighted outer axon diameter (d_A), and is relatively independent of EVF or axon size distribution.

The axonal composition of the CC is expected to differ along its anterior-posterior axis and this appears related to an inherent structure-function relationship facilitating connections to different left/right cortical regions (Frederiksen, 2013; Tzourio-Mazoyer, 2016; van der Knaap and van der Ham, 2011). Based on the simulations presented here and the correlations of larger axon diameters in ex vivo spinal cord with oscillation frequency (i.e. shorter diffusion time) (Xu et al., 2016), our experimental observation of short diffusion time dependency implies that d_A is greater in the genu and splenium than in the body. However, this does not fit with the light microscopy reports from autopsy human CC of a greater number of larger axons in the body (Aboitiz and Montiel, 2003; Aboitiz et al., 1992). In those papers, the genu and splenium are suggested to have more small, densely packed axons with the splenium having some heterogeneity with large axons. Several previous diffusion MRI studies (not OGSE) of the human CC have reported similarities of greater axon density and smaller axons size between the genu and splenium, with the body being different (Alexander et al., 2010; De Santis et al., 2016; Fick et al., 2016; Huang et al., 2015). Our OGSE data does suggest congruence between the genu and splenium, but it is at odds with the body. Other MRI metrics such as g-ratio and relaxation rates also show genu/splenium similarities (smaller g-ratio, R1, and R2) with the body differing in human CC (Björnholm et al., 2017; Thapaliya et al., 2018). T1 has also been shown to vary progressively from anterior to posterior in human CC showing different properties in the genu, body, and splenium rather than having a bookend pattern (Harkins et al., 2016; Lee et al., 2019a).

The lack of OGSE-PGSE diffusivity differences in the body was fairly consistent over all 20 volunteers (male and female, Fig. 3), but, as mentioned above, the reasons for this are unclear given the histology literature. One technical possibility is that the body may be more difficult to measure since it is thinner relative to the axial slice orientations than either the genu or splenium, and may be more prone to image artifacts (e.g. Gibbs ringing), CSF partial volume, and pulsatility effects that differ between OGSE and PGSE waveforms (Baron and Beaulieu, 2014; Wu and Zhang, 2017). Regions located at the center of the brain and around the body of the corpus callosum are more sensitive to cardiac pulsation artifacts in DTI (Chung et al., 2010). There are several individuals where the body CC showed greater diffusivity values on the longer diffusion time PGSE, relative to OGSE, which is not congruent with what is expected physically. Our previous tractography based analysis on a subset of the cohort found no changes in the body CC for axial and radial diffusivities at short diffusion times, but there was an FA reduction (Baron and Beaulieu, 2014); note that we do observe a small FA reduction with OGSE in the body CC of females here. Overall, the lack of OGSE-PGSE diffusivity differences in the body requires verification with higher image spatial resolution with minimal CSF contamination and other artifacts.

The experimental OGSE-PGSE RD difference of 0.04–0.10 $\times$ 10^{-3} mm^2/s (5–20%) between OGSE and PGSE in the genu/splenium corresponds to d_A = 3–6 μm from simulations. This agrees well with the mean inner axon diameter that Alexander et al. report in their simulations (based on the Aboitiz et al., 1992 paper) of 2–5 μm, whereas the axon diameter mapping gave larger estimates of 6–14 μm (see Fig. 9, left panel in (Alexander et al., 2010)). The ability to distinguish smaller axons can be improved with stronger gradients, although previous PGSE studies used longer diffusion times than the 4 ms used here with OGSE (Drobnjak et al., 2016; Dyrby et al., 2013; Huang et al., 2015; Nilsson et al., 2017). The early autopsy studies suggest that the majority of inner axon diameters in human brain are <1 μm, so our outer diameter axon values of 3–6 μm may seem erroneously large. However all histology approaches include underestimation of axon diameters up to 50% due to fixation shrinkage (Marner et al., 2003). Electron microscopy of human CC revealed a range of inner axon diameters from 0.2 to 5 μm (the larger axons were found in the splenium) (Liewald et al., 2014), and this matches recent 3D electron microscopy of mouse CC genu that reported a range of inner axon diameters from 0.3 to 3 μm (Lee et al., 2019b). Furthermore, although not reported in the Aboitiz et al., 1992 paper (Aboitiz et al., 1992), our estimate of axon area based on their Fig. 1 suggests that the axons greater than 1 μm contribute about 60% of the axon area, despite their much smaller numbers, and hence for diffusion MRI these contribute to 60% of the water signal (ignoring relaxation, etc.). Thus, a small proportion of larger axons could drive an OGSE-PGSE difference. An illustrative example of this is shown in Fig. 9 where the addition of only 1% of axons with 12 μm outer diameter increases the area-weighted axon diameter by 2.3x (i.e. from 2.4 to 5.6 μm) with almost no change in mean diameter (i.e. from 1.5 to 1.6 μm). By cross-referencing this with our simulations in Fig. 7B, the RD OGSE-PGSE difference would go from ~0.02 $\times$ 10^{-3} mm^2/s to ~0.10 $\times$ 10^{-3} mm^2/s.

Sex differences have not been considered previously in animal OGSE versus PGSE central nervous system studies (Aggarwal et al., 2012; Kershaw et al., 2013; Pyatigorskaya et al., 2014; Xu et al., 2014) nor in human brain studies, which were primarily a demonstration of the feasibility of these methods in human brain and had limited sample size (Baron and Beaulieu, 2014; Van et al., 2014). Here males and females showed comparable short diffusion time changes in the splenium and comparable no changes in the body, but males did show greater change in the genu. The OGSE-PGSE RD of the genu increased by 22% in males whereas it was only 5% in females. This suggests that males on average have larger area-weighted axon diameter in the genu CC. Testosterone-dependent axon diameter has been shown in the rat splenium, but other CC regions were not assessed (Pesaresi et al., 2015). We did not see sex differences of diffusion time dependence in the human splenium CC however. Ultrastructural analysis of an in vitro model of rat and human axons has shown that males had considerably larger axons than females (Dolle et al., 2018).

An increase of OGSE - PGSE differences with aging over 21–73 years was observed in female participants in all CC sub-regions for at least one diffusivity parameter. Given that greater OGSE-PGSE differences are related to larger axon diameters (Xu et al., 2016) or area-weighted axon outer diameters in our simulations, this difference suggests reorganization in white matter axonal content such as loss of smaller axons leading to a larger mean axon diameter. These observations appear to be in accordance with various animal histology studies in female rats (Yang et al., 2009) (no male rats were included in that study) and both male and female rhesus monkey (Bowley et al., 2010) that showed a marked loss of smaller axons in white matter with aging. This was also seen in human autopsy studies where female (Tang et al., 1997) (no males were included in that study) or both sexes (Marner et al., 2003) showed loss of small diameter axons with aging. These histology studies are supported by a combined multi-shell diffusion/quantitative magnetization transfer MRI study showing an increase of g-ratio with aging for combined males and females across several white matter tracts (Cercignani et al., 2017), since smaller axons tend to have lower g-ratios. When looking specifically at the corpus callosum, one of the first histology studies looking at age relationships showed a higher prevalence of CC axon size correlation with age in females (Aboitiz et al., 1996). A high-gradient (300 mT/m) diffusion (not OGSE) MRI study of the entire CC reported larger axon diameter and lower axon density over ages 22–72 years (n = 36) (Fan et al., 2019). Further subdivisions of the CC suggested larger axon diameters in the genu and lower axon density in the genu and posterior part of the body (Fan et al., 2019). In that study, the age correlations were controlled for gender, but the data was not presented separately for males (n = 13) and females (n = 23), although the majority were female. Our OGSE-PGSE changes with age seem to fit with some of these other observations, but it must be considered exploratory as we have a limited sample size, the significant correlations in females appear to be driven by the three oldest participants at 49, 56 and 73 years old and actual slope differences between males and females are only observed in the body.

Monte Carlo simulations showed that the difference in RD between OGSE and PGSE measurements primarily informs on the area-weighted outer axon diameter, d_A. Individually, the OGSE and PGSE RD measurements were sensitive to EVF, axon diameter distribution shape, and d_A, but the difference in these measures depended primarily on d_A. The relationship between d_A and RD OGSE-PGSE in Fig. 7 is phenomenological, and it is possible that using a measure other than d_A for representative axon size would provide a more informative relationship with RD OGSE-PGSE (see, for example, Supplemental Fig. S1).

Some further insight is gained by breaking out the extra- and intra-axonal signal contributions, as shown in Fig. 8. The corresponding intra-axonal RD OGSE-PGSE difference is essentially zero for $d_A \lesssim 4\ \mu m$, then grows rapidly with increasing d_A. Previous work found that intra-axonal diffusivity depends upon $d_{eff} = (d^6/d^2)^{1/4}$ in the wide pulse limit and $d_{eff} = (d^4/d^2)^{1/2}$ in the narrow pulse limit (Burcaw et al., 2015). Indeed, considering only intra-axonal signals, a plot of RD OGSE-PGSE vs $d_{eff} = (d^6/d^2)^{1/4}$ has less scatter (data not shown) than the corresponding plot vs d_A in Fig. 8B. However, the same is not true when considering the total signal—that is, the data in Fig. 7B is not more parsimoniously represented when plotted vs d_{eff}. This is because, as illustrated in Fig. 8, the diffusion of extra-axonal water dominates RD OGSE-PGSE in the range of axon sizes relevant for this study. While several studies have previously noted a linear relationship between extra-axonal ADC and frequency of the OGSE waveform (Ginsburger et al., 2018; Novikov et al., 2014; Xu et al., 2014), these simulations also suggest that, over the 0–12 μm domain d_A, the extra-axonal RD OGSE-PGSE changes approximately linearly with d_A. Further simulation studies to explore these relationships are ongoing. Note that d_A can be strongly influenced from a small number of large axons (see example, Fig. 9), which are known to be present in human brain at least to a 9–15 μm range based on histology (Aboitiz et al., 1992; Liewald et al., 2014). Thus, it is conceivable that the RD OGSE-PGSE measurement is a more sensitive indicator of the presence of some large diameter axons than histological evaluations, which may characterize only a relatively small number of axons.

The dominant role of extra-axonal water on diffusion metrics derived from long diffusion time (hundreds of ms) experiments has been linked to short range disorder in axon packing stemming from axon heterogeneity (Burcaw et al., 2015; De Santis et al., 2016; Fieremans et al., 2016; Lee et al., 2018; Novikov et al., 2014). Our simulations were limited in terms of tissue complexity, so it is possible that other tissue characteristics are also important in determining this RD difference. For example, the g-ratio was set to be a constant value of 0.7 here, but it is known to vary across axons (Berthold et al., 1983; Chatzopoulou et al., 2008; Crawford et al., 2010). Also, the 2D simulations did not account for axon fiber orientation dispersion, any sources other than the outer membrane for extra-axonal water restriction (e.g., glial cells), myelin water, or possible inter-compartmental water exchange. The 2D simulations also do not yield any axial diffusivity (AD) measures although we showed short diffusion time changes of AD, and others have reported long diffusion time changes of AD in human white matter (Fieremans et al., 2016).

5. Conclusion

White matter microstructure inferences by diffusion MRI is complex, but there is a critical role to play for diffusion time (see review by (Novikov et al., 2019)). Here, short diffusion time OGSE DTI implies differences in the scale of restrictive influences along the human corpus callosum with sex and aging. Future work will need to focus on improving the fidelity of the OGSE/PGSE images and data, as well as examining whole brain for potential differences across various white matter tracts.

Author contributions

Pascal Tétreault: Conceptualization, Methodology, Data Curation, Formal analysis, Investigation, Resources, Writing - Original Draft, Visualization. Kevin D. Harkins: Methodology, Formal analysis, Writing - Review & Editing, Visualization. Corey A. Baron: Resources, Data Curation. Rob Stobbe: Resources, Data Curation. Mark D. Does: Writing - Review & Editing, Supervision, Project administration. Christian Beaulieu: Conceptualization, Writing - Original Draft, Supervision, Project administration, Funding acquisition.

Funding

This work was supported by Canadian Institutes of Health Research (CIHR) and the Canada Research Chairs program (salary award to CB). PT was funded by a postdoctoral fellowship award from CIHR.

Declaration of competing interest

None.

Appendix A. Supplementary data

Supplementary data to this article can be found online at https://doi.org/10.1016/j.neuroimage.2020.116533.

References

Aboitiz, F., Montiel, J., 2003. One hundred million years of interhemispheric communication: the history of the corpus callosum. Braz. J. Med. Biol. Res. 36, 409–420. Revista brasileira de pesquisas médicas e biológicas/Sociedade Brasileira de Biofísica ... [et al.].

Aboitiz, F., Rodríguez, E., Olivares, R., Zaidel, E., 1996. Age-related changes in fibre composition of the human corpus callosum: sex differences. Neuroreport 7, 1761–1764.

Aboitiz, F., Scheibel, A.B., Fisher, R.S., Zaidel, E., 1992. Fiber composition of the human corpus callosum. Brain Res. 598, 143–153.

Aggarwal, M., Jones, M.V., Calabresi, P.A., Mori, S., Zhang, J., 2012. Probing mouse brain microstructure using oscillating gradient diffusion MRI. Magn. Reson. Med. 67, 98–109.
Alexander, D.C., Hubbard, P.L., Hall, M.G., Moore, E.A., Ptito, M., Parker, G.J.M., Dyrby, T.B., 2010. Orientationally invariant indices of axon diameter and density from diffusion MRI. Neuroimage 52, 1374–1389.
Assaf, Y., Blumenfeld-Katzir, T., Yovel, Y., Basser, P.J., 2008. AxCaliber: a method for measuring axon diameter distribution from diffusion MRI. Magn. Reson. Med. 59, 1347–1354.
Barazany, D., Basser, P.J., Assaf, Y., 2009. In vivo measurement of axon diameter distribution in the corpus callosum of rat brain. Brain 132, 1210–1220.
Baron, C.A., Beaulieu, C., 2014. Oscillating gradient spin-echo (OGSE) diffusion tensor imaging of the human brain. Magn. Reson. Med. 72, 726–736.
Beaulieu, C., Allen, P.S., 1996. An in vitro evaluation of the effects of local magnetic-susceptibility-induced gradients on anisotropic water diffusion in nerve. Magn. Reson. Med. 36, 39–44.
Berthold, C.H., Nilsson, I., Rydmark, M., 1983. Axon diameter and myelin sheath thickness in nerve fibres of the ventral spinal root of the seventh lumbar nerve of the adult and developing cat. J. Anat. 136, 483–508.
Björnholm, L., Nikkinen, J., Kiviniemi, V., Nordström, T., Niemelä, S., Drakesmith, M., Evans, J.C., Pike, G.B., Veijola, J., Paus, T., 2017. Structural properties of the human corpus callosum: multimodal assessment and sex differences. Neuroimage 152, 108–118.
Bowley, M.P., Cabral, H., Rosene, D.L., Peters, A., 2010. Age changes in myelinated nerve fibers of the cingulate bundle and corpus callosum in the rhesus monkey. J. Comp. Neurol. 518, 3046–3064.
Burcaw, L.M., Fieremans, E., Novikov, D.S., 2015. Mesoscopic structure of neuronal tracts from time-dependent diffusion. Neuroimage 114, 18–37.
Buzsaki, G., Mizuseki, K., 2014. The log-dynamic brain: how skewed distributions affect network operations. Nat. Rev. Neurosci. 15, 264–278.
Caminiti, R., Carducci, F., Piervincenzi, C., Battaglia-Mayer, A., Confalone, G., Visco-Comandini, F., Pantano, P., Innocenti, G.M., 2013. Diameter, length, speed, and conduction delay of callosal axons in macaque monkeys and humans: comparing data from histology and magnetic resonance imaging diffusion tractography. J. Neurosci. 33, 14501–14511.
Cercignani, M., Giulietti, G., Dowell, N.G., Gabel, M., Broad, R., Leigh, P.N., Harrison, N.A., Bozzali, M., 2017. Characterizing axonal myelination within the healthy population: a tract-by-tract mapping of effects of age and gender on the fiber g-ratio. Neurobiol. Aging 49, 109–118.
Chatzopoulou, E., Miguez, A., Savvaki, M., Levasseur, G., Muzerelle, A., Muriel, M.P., Goureau, O., Watanabe, K., Goutebroze, L., Gaspar, P., Zalc, B., Karagogeos, D., Thomas, J.L., 2008. Structural requirement of TAG-1 for retinal ganglion cell axons and myelin in the mouse optic nerve. J. Neurosci. 28, 7624–7636.
Chomiak, T., Hu, B., 2009. What is the optimal value of the g-ratio for myelinated fibers in the rat CNS? A theoretical approach. PLoS One 4, e7754.
Chung, S., Courcot, B., Sdika, M., Moffat, K., Rae, C., Henry, R.G., 2010. Bootstrap quantification of cardiac pulsation artifact in DTI. Neuroimage 49, 631–640.
Crawford, D.K., Mangiardi, M., Song, B., Patel, R., Du, S., Sofroniew, M.V., Voskuhl, R.R., Tiwari-Woodruff, S.K., 2010. Oestrogen receptor beta ligand: a novel treatment to enhance endogenous functional remyelination. Brain 133, 2999–3016.
De Santis, S., Jones, D.K., Roebroeck, A., 2016. Including diffusion time dependence in the extra-axonal space improves in vivo estimates of axonal diameter and density in human white matter. Neuroimage 130, 91–103.
Does, M.D., Parsons, E.C., Gore, J.C., 2003. Oscillating gradient measurements of water diffusion in normal and globally ischemic rat brain. Magn. Reson. Med. 49, 206–215.
Dolle, J.P., Jaye, A., Anderson, S.A., Ahmadzadeh, H., Shenoy, V.B., Smith, D.H., 2018. Newfound sex differences in axonal structure underlie differential outcomes from in vitro traumatic axonal injury. Exp. Neurol. 300, 121–134.
Drobnjak, I., Zhang, H., Ianuş, A., Kaden, E., Alexander, D.C., 2016. PGSE, OGSE, and sensitivity to axon diameter in diffusion MRI: insight from a simulation study. Magn. Reson. Med. 75, 688–700.
Dyrby, T.B., Sogaard, L.V., Hall, M.G., Ptito, M., Alexander, D.C., 2013. Contrast and stability of the axon diameter index from microstructure imaging with diffusion MRI. Magn. Reson. Med. 70, 711–721.
Fan, Q., Nummenmaa, A., Wichtmann, B., Witzel, T., Mekkaoui, C., Schneider, W., Wald, L.L., Huang, S.Y., 2018. Validation of diffusion MRI estimates of compartment size and volume fraction in a biomimetic brain phantom using a human MRI scanner with 300mT/m maximum gradient strength. Neuroimage 182, 469–478.
Fan, Q., Tian, Q., Ohringer, N.A., Nummenmaa, A., Witzel, T., Tobyne, S.M., Klawiter, E.C., Mekkaoui, C., Rosen, B.R., Wald, L.L., Salat, D.H., Huang, S.Y., 2019. Age-related alterations in axonal microstructure in the corpus callosum measured by high-gradient diffusion MRI. Neuroimage 191, 325–336.
Fick, R.H.J., Wassermann, D., Caruyer, E., Deriche, R., 2016. MAPL: tissue microstructure estimation using Laplacian-regularized MAP-MRI and its application to HCP data. Neuroimage 134, 365–385.
Fieremans, E., Burcaw, L.M., Lee, H.-H., Lemberskiy, G., Veraart, J., Novikov, D.S., 2016. In vivo observation and biophysical interpretation of time-dependent diffusion in human white matter. Neuroimage 129, 414–427.
Frederiksen, K.S., 2013. Corpus callosum in aging and dementia. Dan Med J 60, B4721.
Ginsburger, K., Poupon, F., Beaujoin, J., Estournet, D., Matuschke, F., Mangin, J.-F., Axer, M., Poupon, C., 2018. Improving the realism of white matter numerical phantoms: a step toward a better understanding of the influence of structural disorders in diffusion MRI. Front. Phys. 6.
Hall, M.G., Alexander, D.C., 2009. Convergence and parameter choice for Monte-Carlo simulations of diffusion MRI. IEEE Trans. Med. Imaging 28, 1354–1364.
Harkins, K.D., Does, M.D., 2016. Simulations on the influence of myelin water in diffusion-weighted imaging. Phys. Med. Biol. 61, 4729–4745.
Harkins, K.D., Xu, J., Dula, A.N., Li, K., Valentine, W.M., Gochberg, D.F., Gore, J.C., Does, M.D., 2016. The microstructural correlates of T1 in white matter. Magn. Reson. Med. 75, 1341–1345.
Huang, S.Y., Nummenmaa, A., Witzel, T., Duval, T., Cohen-Adad, J., Wald, L.L., McNab, J.A., 2015. The impact of gradient strength on in vivo diffusion MRI estimates of axon diameter. Neuroimage 106, 464–472.
Kakkar, L.S., Bennett, O.F., Siow, B., Richardson, S., Ianus, A., Quick, T., Atkinson, D., Phillips, J.B., Drobnjak, I., 2018. Low frequency oscillating gradient spin-echo sequences improve sensitivity to axon diameter: an experimental study in viable nerve tissue. Neuroimage 182, 314–328.
Kershaw, J., Leuze, C., Aoki, I., Obata, T., Kanno, I., Ito, H., Yamaguchi, Y., Handa, H., 2013. Systematic changes to the apparent diffusion tensor of in vivo rat brain measured with an oscillating-gradient spin-echo sequence. Neuroimage 70, 10–20.
Klein, S., Staring, M., Murphy, K., Viergever, M.A., Pluim, J.P., 2010. elastix: a toolbox for intensity-based medical image registration. IEEE Trans. Med. Imaging 29, 196–205.
Lee, B.Y., Zhu, X.H., Li, X., Chen, W., 2019a. High-resolution imaging of distinct human corpus callosum microstructure and topography of structural connectivity to cortices at high field. Brain Struct. Funct. 224, 949–960.
Lee, H.H., Fieremans, E., Novikov, D.S., 2018. What dominates the time dependence of diffusion transverse to axons: intra- or extra-axonal water? Neuroimage 182, 500–510.
Lee, H.H., Yaros, K., Veraart, J., Pathan, J.L., Liang, F.X., Kim, S.G., Novikov, D.S., Fieremans, E., 2019b. Along-axon diameter variation and axonal orientation dispersion revealed with 3D electron microscopy: implications for quantifying brain white matter microstructure with histology and diffusion MRI. Brain Struct. Funct. 224, 1469–1488.
Leemans, A., Jones, D.K., 2009. The B-matrix must be rotated when correcting for subject motion in DTI data. Magn. Reson. Med. 61, 1336–1349.
Lemberskiy, G., Baete, S.H., Cloos, M.A., Novikov, D.S., Fieremans, E., 2017. Validation of surface-to-volume ratio measurements derived from oscillating gradient spin echo on a clinical scanner using anisotropic fiber phantoms. NMR Biomed. 30, e3708.
Liewald, D., Miller, R., Logothetis, N., Wagner, H.-J., Schüz, A., 2014. Distribution of axon diameters in cortical white matter: an electron-microscopic study on three human brains and a macaque. Biol. Cybern. 108, 541–557.
Lundell, H., Sonderby, C.K., Dyrby, T.B., 2015. Diffusion weighted imaging with circularly polarized oscillating gradients. Magn. Reson. Med. 73, 1171–1176.
Marner, L., Nyengaard, J.R., Tang, Y., Pakkenberg, B., 2003. Marked loss of myelinated nerve fibers in the human brain with age. J. Comp. Neurol. 462, 144–152.
Niendorf, T., Norris, D.G., Leibfritz, D., 1994. Detection of apparent restricted diffusion in healthy rat brain at short diffusion times. Magn. Reson. Med. 32, 672–677.
Nilsson, M., Lasič, S., Drobnjak, I., Topgaard, D., Westin, C.-F., 2017. Resolution limit of cylinder diameter estimation by diffusion MRI: the impact of gradient waveform and orientation dispersion. NMR Biomed. 30, e3711.
Novikov, D.S., Fieremans, E., Jespersen, S.N., Kiselev, V.G., 2019. Quantifying brain microstructure with diffusion MRI: theory and parameter estimation. NMR Biomed. 32, e3998.
Novikov, D.S., Jensen, J.H., Helpern, J.A., Fieremans, E., 2014. Revealing mesoscopic structural universality with diffusion. Proc. Natl. Acad. Sci. U. S. A. 111, 5088–5093.
Novikov, D.S., Kiselev, V.G., 2010. Effective medium theory of a diffusion-weighted signal. NMR Biomed. 23, 682–697.
Parsons, E.C., Does, M.D., Gore, J.C., 2003. Modified oscillating gradient pulses for direct sampling of the diffusion spectrum suitable for imaging sequences. Magn. Reson. Imag. 21, 279–285.
Perrone, D., Aelterman, J., Pizurica, A., Jeurissen, B., Philips, W., Leemans, A., 2015. The effect of Gibbs ringing artifacts on measures derived from diffusion MRI. Neuroimage 120, 441–455.
Pesaresi, M., Soon-Shiong, R., French, L., Kaplan, D.R., Miller, F.D., Paus, T., 2015. Axon diameter and axonal transport: in vivo and in vitro effects of androgens. Neuroimage 115, 191–201.
Portnoy, S., Flint, J.J., Blackband, S.J., Stanisz, G.J., 2013. Oscillating and pulsed gradient diffusion magnetic resonance microscopy over an extended b-value range: implications for the characterization of tissue microstructure. Magn. Reson. Med. 69, 1131–1145.
Pyatigorskaya, N., Le Bihan, D., Reynaud, O., Ciobanu, L., 2014. Relationship between the diffusion time and the diffusion MRI signal observed at 17.2 Tesla in the healthy rat brain cortex. Magn. Reson. Med. 72, 492–500.
Schachter, M., Does, M.D., Anderson, A.W., Gore, J.C., 2000. Measurements of restricted diffusion using an oscillating gradient spin-echo sequence. J. Magn. Reson. 147, 232–237.
Sepehrband, F., Alexander, D.C., Kurniawan, N.D., Reutens, D.C., Yang, Z., 2016. Towards higher sensitivity and stability of axon diameter estimation with diffusion-weighted MRI. NMR Biomed. 29, 293–308.
Shamonin, D.P., Bron, E.E., Lelieveldt, B.P., Smits, M., Klein, S., Staring, M., 2013. Fast parallel image registration on CPU and GPU for diagnostic classification of Alzheimer's disease. Front. Neuroinf. 7, 50. Alzheimer's Disease Neuroimaging, I.
Shemesh, N., Alvarez, G.A., Frydman, L., 2013. Measuring small compartment dimensions by probing diffusion dynamics via Non-uniform Oscillating-Gradient Spin-Echo (NOGSE) NMR. J. Magn. Reson. 237, 49–62.
Shemesh, N., Alvarez, G.A., Frydman, L., 2015. Size distribution imaging by non-uniform oscillating-gradient spin echo (NOGSE) MRI. PLoS One 10, e0133201.
Stahon, K.E., Bastian, C., Griffith, S., Kidd, G.J., Brunet, S., Baltan, S., 2016. Age-related changes in axonal and mitochondrial ultrastructure and function in white matter. J. Neurosci. 36, 9990–10001.

Stanisz, G.J., Szafer, A., Wright, G.A., Henkelman, R.M., 1997. An analytical model of restricted diffusion in bovine optic nerve. Magn. Reson. Med. 37, 103–111.
Stikov, N., Campbell, J.S.W., Stroh, T., Lavelée, M., Frey, S., Novek, J., Nuara, S., Ho, M.-K., Bedell, B.J., Dougherty, R.F., Leppert, I.R., Boudreau, M., Narayanan, S., Duval, T., Cohen-Adad, J., Picard, P.-A., Gasecka, A., Côté, D., Pike, G.B., 2015. In vivo histology of the myelin g-ratio with magnetic resonance imaging. Neuroimage 118, 397–405.
Szafer, A., Zhong, J., Gore, J.C., 1995. Theoretical model for water diffusion in tissues. Magn. Reson. Med. 33, 697–712.
Tang, Y., Nyengaard, J.R., Pakkenberg, B., Gundersen, H.J., 1997. Age-induced white matter changes in the human brain: a stereological investigation. Neurobiol. Aging 18, 609–615.
Tanner, J.E., 1979. Self diffusion of water in frog muscle. Biophys. J. 28, 107–116.
Thapaliya, K., Vegh, V., Bollmann, S., Barth, M., 2018. Assessment of microstructural signal compartments across the corpus callosum using multi-echo gradient recalled echo at 7 T. Neuroimage 182, 407–416.
Tzourio-Mazoyer, N., 2016. Intra- and inter-hemispheric connectivity supporting hemispheric specialization. In: Kennedy, H., Van Essen, D.C., Christen, Y. (Eds.), Micro-, Meso- and Macro-Connectomics of the Brain, Cham (CH), pp. 129–146.
Van, A.T., Holdsworth, S.J., Bammer, R., 2014. In vivo investigation of restricted diffusion in the human brain with optimized oscillating diffusion gradient encoding. Magn. Reson. Med. 71, 83–94.
van der Knaap, L.J., van der Ham, I.J., 2011. How does the corpus callosum mediate interhemispheric transfer? A review. Behav. Brain Res. 223, 211–221.
Wu, D., Zhang, J., 2017. The effect of microcirculatory flow on oscillating gradient diffusion MRI and diffusion encoding with dual-frequency orthogonal gradients (DEFOG). Magn. Reson. Med. 77, 1583–1592.
Xu, J., Li, H., Harkins, K.D., Jiang, X., Xie, J., Kang, H., Does, M.D., Gore, J.C., 2014. Mapping mean axon diameter and axonal volume fraction by MRI using temporal diffusion spectroscopy. Neuroimage 103, 10–19.
Xu, J., Li, H., Li, K., Harkins, K.D., Jiang, X., Xie, J., Kang, H., Dortch, R.D., Anderson, A.W., Does, M.D., 2016. Fast and simplified mapping of mean axon diameter using temporal diffusion spectroscopy. NMR Biomed. 29, 400–410.
Yang, S., Li, C., Lu, W., Zhang, W., Wang, W., Tang, Y., 2009. The myelinated fiber changes in the white matter of aged female Long-Evans rats. J. Neurosci. Res. 87, 1582–1590.